A Simplified Design Method for Quasi Resonant Inverter Used in Induction Hob

Metin Ozturk *

Posted Date: 29 August 2023

doi: 10.20944/preprints202308.1905.v1

Keywords: Home appliances; induction cooking systems; induction cooker design; resonant converter circuit parameters; single switch quasi resonant inverter

Article

A Simplified Design Method for Quasi Resonant Inverter Used in Induction Hob

Metin Ozturk [1,2]

[1] Department of Electrical and Electronics Engineering, Istanbul Esenyurt University, 34510 Istanbul, Turkey; metinozturk@esenyurt.edu.tr; Tel.: +90 535 5050430.

[2] Department of Research and Development, Mamur Technology Systems Inc, 34590 Istanbul, Turkey;

Abstract: Induction heating (IH) technology is widely recognized and utilized in residential applications due to its high efficiency and safe operating characteristics. Resonant inverter circuits are widely used in IH systems because of their high efficiency and ability to perform soft-switching. Among the various resonant inverters used in IH systems, the single-switch quasi-resonant (SSQR) inverter topology is typically preferred for low-cost and low-output-power applications. Despite its cost advantage, the SSQR topology has a relatively narrow soft-switching range, which can be unstable depending on the electrical parameters of the load and the resonant converter circuit. Accurately determining the capacitance value of the resonant capacitor and the inductance value of the induction coil, which are the key circuit elements of the SSQR induction cooker, is crucial for designing a reliable, efficient, and durable cooking system. In other words, there exists a critical relationship between the resonant converter circuit parameters, load characteristics, and safe operating conditions. Additionally, when considering closed-loop control methods used for power control and safety, selecting appropriate resonant circuit elements becomes vital in ensuring both reliable and efficient operation. This paper focuses on a novel and simplified design method for the SSQR inverter utilized in household appliances. The proposed method and its advantages in terms of the safe operating area of the switch are theoretically investigated and verified through simulations and prototype circuits.

Keywords: home appliances; induction cooking systems; induction cooker design; resonant converter circuit parameters; single switch quasi resonant inverter

1. Introduction

Induction heating systems have gained significant popularity in industrial, domestic, and medical applications over the past few decades due to their notable features including user safety, efficient and rapid heating, and easy maintenance [1–4]. The advancements in power electronics as well as electronics have contributed to the progress of induction technology [5–8]. In domestic induction cooking appliances, one or more induction coils are positioned beneath a vitro ceramic glass surface to heat up pans placed on top of it [9–11]. The induction coil is supplied with an alternating current, generating a magnetic field at the same frequency as the coil current in order to heat the pan. This heating process occurs through the induction surface by inducing eddy currents in the pan [2,12]. The main components of induction heating systems consist of a rectifier unit for AC-DC conversion and resonant inverter units [13,14]. Figure 1 illustrates a general power-transfer loop for domestic appliances.

Preprints (www.preprints.org) | NOT PEER-REVIEWED | Posted: 29 August 2023 doi:10.20944/preprints202308.1905.v1

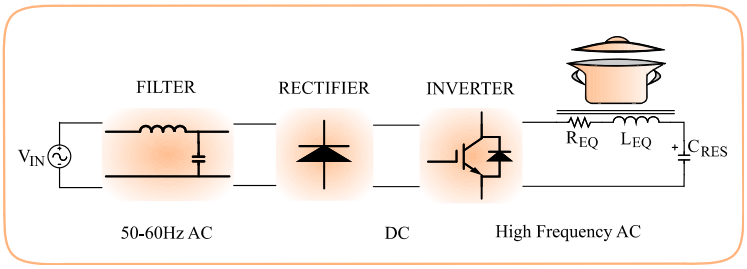

Figure 1. General power transfer loop.

Power converters, which are a crucial component of Induction heating systems, employ either single-stage or double-stage structures [15]. Double-stage systems involve both AC to DC and DC to AC conversions within IH systems [13,14]. In contrast, single-stage AC to AC systems lack a rectifier stage. These systems can be categorized into two groups: those that directly convert the input AC voltage and those that boost it.

Furthermore, Induction heating systems are composed of either single or multiple loads/coils. In the past years, single coil systems have been extensively utilized in both industrial and domestic induction applications. Recent advancements in multiple output induction heaters suggest enhancing performance through adjustable cooking surfaces [16–18]. The selection of different coil models depends on factors such as design requirements, cost, output power, and hob geometry. Various approaches are employed to configure cooking surfaces based on the pan size and coil design [16,19]. While pans made of ferromagnetic material are commonly used as loads, recent studies have also explored heating pans made of all metal materials [20–24].

Different resonant inverter topologies have been proposed based on the trade-off between cost and performance, which needs to be evaluated for each specific application. The most common inverter topologies in induction heating (IH) systems are half-bridge series resonant (HBSR) [25–28] and single-switch quasi-resonant (SSQR) [29–31] inverters. The SSQR inverter topology provides a reliable solution for low-power and low-cost IH applications. However, the main drawback of the quasi-resonant inverter circuit is its inability to control the power transferred to the load in a frequency-controlled manner, as in HBSR inverter circuits. This limitation stems from the fact that the working modes of the SSQR inverter switch between RL and RLC circuits [11,32]. Consequently, closed-loop control algorithms are employed to determine the turn-on and turn-off times of the semiconductor switch.

In IH systems utilizing SSQR inverters, a significant correlation exists among the resonant converter circuit, load parameters, current and voltage limits of the semiconductor switch, turn-on and turn-off times of the semiconductor switch, and closed-loop power control methodologies. Furthermore, when assessed in conjunction with the closed-loop control techniques employed for power regulation and safety purposes, the selection of resonant circuit elements assumes critical importance in guaranteeing a reliable and efficient operation.

Coil equivalent inductance and resistance values, which form the electrical model of the system comprising the coil and the pan, are challenging to determine during the modeling of resonant circuit elements. Additionally, these values are subject to variations based on factors such as the operating frequency of the resonant circuit, ambient temperature, and air gap between the pan and the coil. As a result, there exists a wide range of academic research focusing on pan and load recognition [11,29,33–36]. However, the design of the coil itself necessitates a comprehensive academic investigation. Numerous studies have been conducted on coil design, particularly in the context of magnetic fields [37–39].

The wide range of electrical loads associated with pans used in domestic induction hob applications with SSQR inverters allows for customization of the electrical circuit parameters based on user preferences. Furthermore, the heat generated in the pan affects the values of circuit variables such as resistance and inductance, and potential variations due to the electrical network necessitate certain assumptions to be made in the design of the heating system with SSQR inverter.

Preprints (www.preprints.org) | NOT PEER-REVIEWED | Posted: 29 August 2023 doi:10.20944/preprints202308.1905.v1

In [40,41], a Class E inverter design utilizing one inductor and one capacitor is presented. During the initial stages of the design, semiconductor losses are disregarded, and it is assumed that the pan resistance remains constant. Additionally, the coil design precedes the circuit design, and the equivalent inductance (L) and equivalent resistance (R) values are determined based on the operating frequency (f). Similarly, in [42], prior to the implementation of the related design, the input voltage (V_S), work coil parameters (Q, R_L, L_R), water mass (m), and required boiling time (t) must be defined. In [43], the design process requires the specification of inverter output power (P), DC input voltage (U_{DC}), resonant frequency (f), as well as various other load and coil parameters. In [44], the inductance value is calculated based on the number of turns N, wire diameter W, and space S between consecutive turns. In [45], the finite-element method is employed, utilizing the coil's geometry. It is noted that the inductance value varies due to the physical interaction between the coil and the ferromagnetic pan; however, there is no provided data regarding the specific inductance value for the pan.

As a result, the studies briefly mentioned above require that critical information such as coil geometry, coil design and coil inductance value must be defined before starting the circuit design, by making some assumptions. However, while designing the SSQR inverter system, it is very important to determine the coil inductance value, as in other converter designs. In other words, the purpose of the design is to determine the coil inductance value to be used in the SSQR inverter. Defining a certain value for coil inductance before starting the design will complicate the circuit design process and prolong the process of obtaining output values such as current, voltage and power at desired values.

Also, in practical circuit design applications, using the inductance value as an input parameter may not be as practical as described in the references provided. From this point of view, the proposed method provides a feasible design approach for initial conditions where the critical circuit parameters of the resonant circuit, namely coil inductance L_{EQ}, equivalent circuit resistance R_{EQ} and resonant circuit capacitor value C_{RES} are not known, by utilizing the energy desired to be transferred to the coil inductor.

Input parameters such as the mains input voltage V_{AC}, the output power P to be transferred to the pot and the switching times of the semiconductor are determined before the design phase. Then all circuit parameters including L_{EQ}, R_{EQ} and C_{RES} can be determined using the proposed calculation method. In this way, it is aimed to create a reference method especially for practitioners who are new to SSQR design.

The rest of the manuscript is structured as follows: In Section II, the circuit description of the SSQR inverter converter is explained. In Section III, the detailed proposed design method of SSQR inverter is summarized. Section IV shows the calculation, simulation, and experimental results, respectively. The conclusion of this study is outlined in Section V.

2. Circuit Description

The circuit diagram and schematic of the single-switch quasi-resonant inverter, along with its primary operational waveforms, are presented in Figures 2 and 3, respectively. The circuit schematic comprises a semiconductor switch denoted as T, a freewheeling diode labeled D, an equivalent resistance represented by R_{EQ}, an equivalent inductance designated as L_{EQ}, and a resonance capacitor denoted as C_{RES}. Upon the activation of the T switch, the circuit behaves analogously to a series RL circuit. During this phase, the coil accumulates energy through the resistance R_{EQ} over a duration labeled as t_{ON}. Throughout the turn-on time, the coil accumulates energy provided by the primary voltage source V_{DC}.

Preprints (www.preprints.org) | NOT PEER-REVIEWED | Posted: 29 August 2023 doi:10.20944/preprints202308.1905.v1

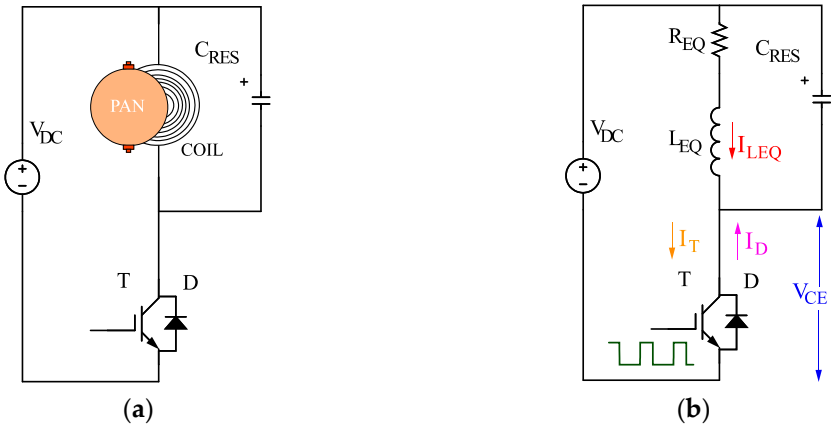

Figure 2. Single switch inverter (a) circuit diagram (b) circuit schematic.

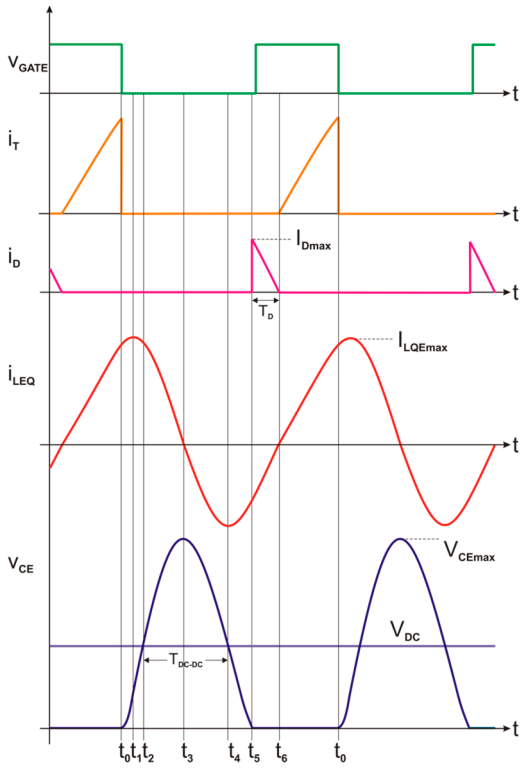

Figure 3. General power transfer loop.

When the T switch is closed, the circuit starts to work as a series RLC circuit. In this configuration, resonance is established between the coil and the capacitor, facilitating energy exchange. The resonance capacitor, C_{RES}, charges to the peak voltage, V_{CEMAX}, and eventually discharges to zero. A short time after the capacitor has completely discharged, the switch is promptly reactivated, in accordance with references [1,46,47].

3.1. Circuit Operating Modes – Waveform Equations

The operational modes of the single-switch resonant inverter, depicted in Figure 4, are examined across four primary operational stages. The conduction period of the T semiconductor, denoted as $t_6 < t < t_0$, is mathematically modeled as a series RL circuit incorporating components R_{EQ} and L_{EQ}. Simultaneously, the time interval $t_0 < t < t_5$, characterized by resonance interactions between L_{EQ} and C_{RES}, is subjected to analysis as a series RLC circuit. Lastly, the conduction duration of the D freewheeling diode, $t_5 < t < t_6$, is depicted through a series RL circuit model. Owing to the behavior of the single-switch resonant inverter as a series RLC circuit during states 2 and 3 among

Preprints (www.preprints.org) | NOT PEER-REVIEWED | Posted: 29 August 2023 doi:10.20944/preprints202308.1905.v1

the four operational states, and as a series RL circuit during states 1 and 4, the associated circuit is evaluated in the time domain as opposed to the frequency domain.

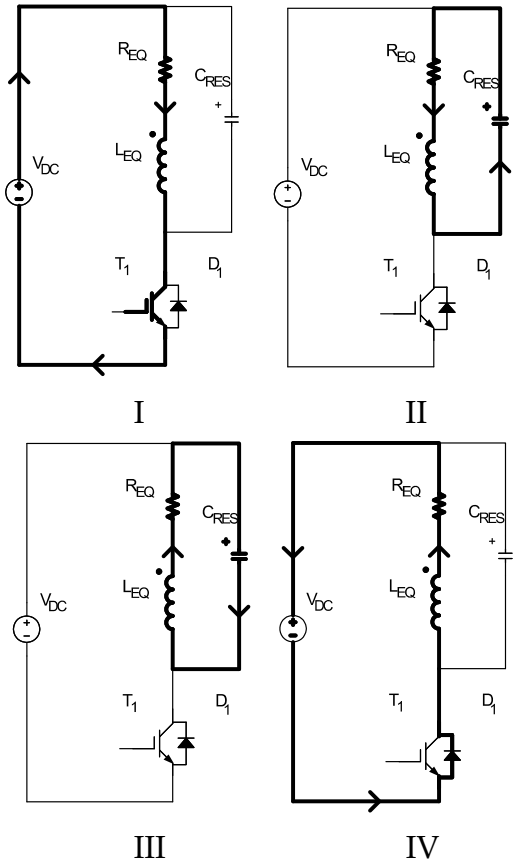

Figure 4. Circuit operating modes of single switch inverter.

Throughout the analysis, particular attention is directed towards steady-state analysis, with a focus on the initial operational stage. Potential phenomena like resonance capacitor discharge current and analogous transient states are deliberately disregarded for the sake of analytical simplicity.

Stage I$(t_6 - t_0)$: This interval commences with the initiation of the T semiconductor under zero voltage conditions (ZVT) and persists until the T switch deactivates. Regarding the operation of the RL circuit, the subsequent equations can be formulated as illustrated in equations (1)-(3).

$$i_{LEQ}(t_6) = 0 \tag{1}$$

$$i_{LEQ}(t) = i_T(t) = \frac{V_{DC}}{R_{LEQ}} \cdot (1 - e^{-\frac{R_{EQ}}{L_{EQ}} \cdot t}) \tag{2}$$

$$V_{DC} = V_{LEQ} + V_{REQ} \tag{3}$$

Stage II-III$(t_0 - t_5)$: This interval initiates with the deactivation of the T semiconductor, and the resonance phenomenon between L_{EQ} and C_{RES} is scrutinized through analysis as a series RLC circuit. Furthermore, the subsequent equations can be established to characterize the current I_{LEQ}, as depicted in equations (4)-(7).

$$i_{LEQ}(t) = e^{-\alpha t}(B_1 cos(\omega_d t) + B_2 sin(\omega_d t)) \tag{4}$$

$$di_{LEQ}(t)/dt = -e^{-\alpha t}[(B_1\omega_d + B_2\alpha)sin(\omega_d t) + (B_1\alpha - B_2\omega_d)cos(\omega_d t)] \tag{5}$$

$$i_{LEQ}(t_0) \Longrightarrow B_1 = I_0 \tag{6}$$

$di_{LEQ}(t_0)/dt \implies$

Preprints (www.preprints.org) | NOT PEER-REVIEWED | Posted: 29 August 2023 doi:10.20944/preprints202308.1905.v1

$$B_2 = ((V_{DC} - R_{EQ}I_0))/(L_{EQ}\omega_d) + (\alpha I_0)/\omega_d \quad (7)$$

Furthermore, the mentioned equations, along with the circuit equations (8)-(11), can be employed to compute the switch collector-emitter voltage V_{CE} as illustrated in Figure 3.

$$v(t) = V_{DC} + e^{-\alpha t}(A_1 cos(\omega_d t) + A_2 sin(\omega_d t)) \quad (8)$$

$$dv(t)/dt = -e^{-\alpha t}[(A_1\omega_d + A_2\alpha)sin(\omega_d t) + (A_1\alpha - A_2\omega_d)cos(\omega_d t)] \quad (9)$$

$$v(t_0) \Longrightarrow A_1 = -V_{DC} \quad (10)$$

$$dv(t_0)/dt \Longrightarrow A_2 = (I_0/C_{RES} - \alpha V_{DC})/\omega_d \quad (11)$$

Stage IV $(t_5 - t_6)$: This interval initiates with the activation of the D diode, which is connected in anti-parallel to the T power switch. As depicted in Figure 3, the dissipation of current or energy through the source is managed by a D power diode. Regarding the operation of the RL circuit, the ensuing equations can be formulated as demonstrated in equations (12)-(15). The duration of diode current conduction, $t_D(t_6 - t_5)$, and the peak diode current are denoted as I_{Dmax}.

$$i_{LEQ}(t) = \frac{V_{DC}}{R_{EQ}} + (I_{Dmax} - \frac{V_{DC}}{R_{EQ}})e^{-\frac{R_{EQ}}{L_{EQ}}t} \quad (12)$$

$$i_{LEQ}(t_D) = 0 = \frac{V_{DC}}{R_{EQ}} + (I_{Dmax} - \frac{V_{DC}}{R_{EQ}})e^{-\frac{R_{EQ}}{L_{EQ}}t_D} \quad (13)$$

$$t_D = \ln[\frac{V_{DC}/R_{EQ}}{V_{DC}/R_{EQ} - I_{Dmax}}](-\frac{L_{EQ}}{R_{EQ}}) \quad (14)$$

$$t_D = -\frac{L_{EQ}}{R_{EQ}} \cdot ln\left(1 + \frac{I_{Dmax}}{V_{DC}/R_{EQ} - I_{Dmax}}\right) \quad (15)$$

3.2. Safe Operating Area for Quasi Resonant Inverter

From the provided first- and second-order circuit equations, it is evident that the precise determination of R_{EQ}, L_{EQ} and C_{RES} values hold paramount importance for ensuring the secure operational conditions of quasi-resonant induction heating applications. The chief threats to safe functionality within power electronic circuits encompass both elevated voltage and current surpassing the maximum operational thresholds of the employed semiconductors. Although all constituents of electronic circuits can be influenced by overcurrent and overvoltage stress, semiconductor switches stand out as the most vulnerable elements in inverter applications. Even if excess heat generated by excessive current can be mitigated through enforced cooling methodologies, semiconductors subjected to voltages surpassing their breakdown thresholds can promptly render them non-operational. By employing the PSpice simulation program, variations in the collector-emitter voltage (V_{CE}) of the semiconductor switch are assessed across diverse resonant circuit parameter configurations, as visually depicted in Figure 5.

Preprints (www.preprints.org) | NOT PEER-REVIEWED | Posted: 29 August 2023 doi:10.20944/preprints202308.1905.v1

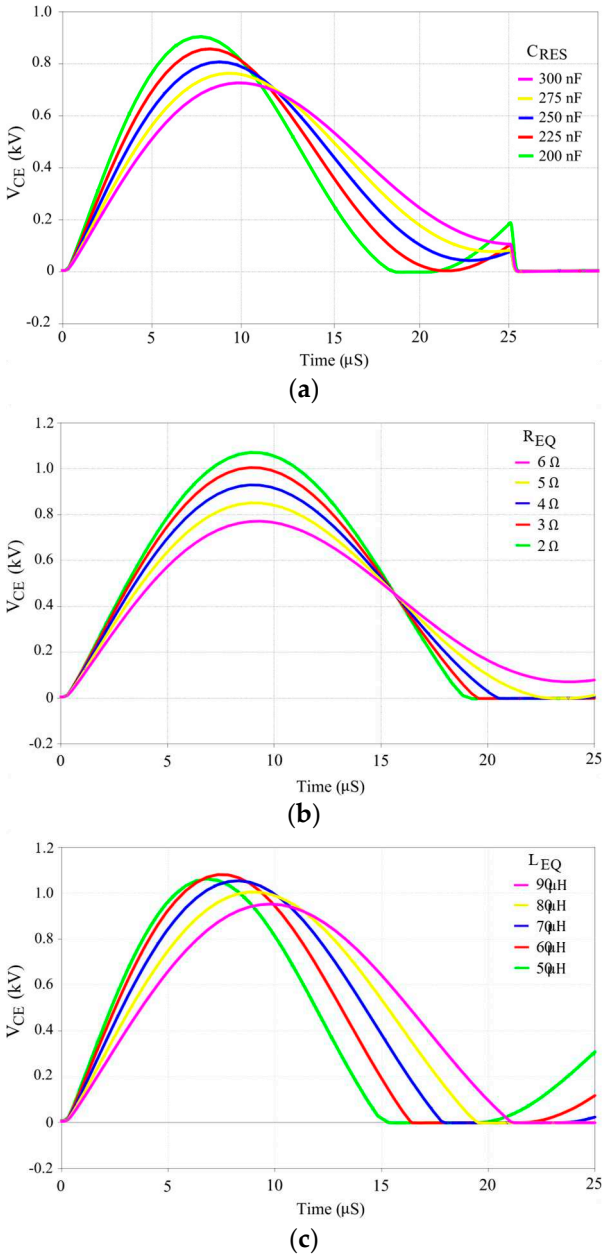

Figure 5. V_{CE} voltage value variances in PSpice. (a) $R_{EQ} = 3\ \Omega$, $L_{EQ} = 80\ \mu H$ and depending on C_{RES} values. (b) $C_{RES} = 270\ nF$, $L_{EQ} = 80\ \mu H$ and depending on R_{EQ} values. (c) $R_{EQ} = 3\ \Omega$, $C_{RES} = 270\ nF$ depending on L_{EQ} values.

Similarly, discharge currents of the C_{RES} capacitor, frequently observed within quasi-resonant inverter circuits, pose a threat to the reliable operational conditions of both semiconductors and power electronics circuits. These instantaneous currents, also referred to as light load currents, can exceed the nominal maximum current of the semiconductor (or coil current I_{LEQ}) by three to four times, resulting in issues such as overheating, stress, and similar challenges. Just like the V_{CE} voltage example, the semiconductor switch current I_T is derived using the PSpice simulation program, contingent upon resonant circuit parameters, as depicted in Figure 6.

Preprints (www.preprints.org) | NOT PEER-REVIEWED | Posted: 29 August 2023 doi:10.20944/preprints202308.1905.v1

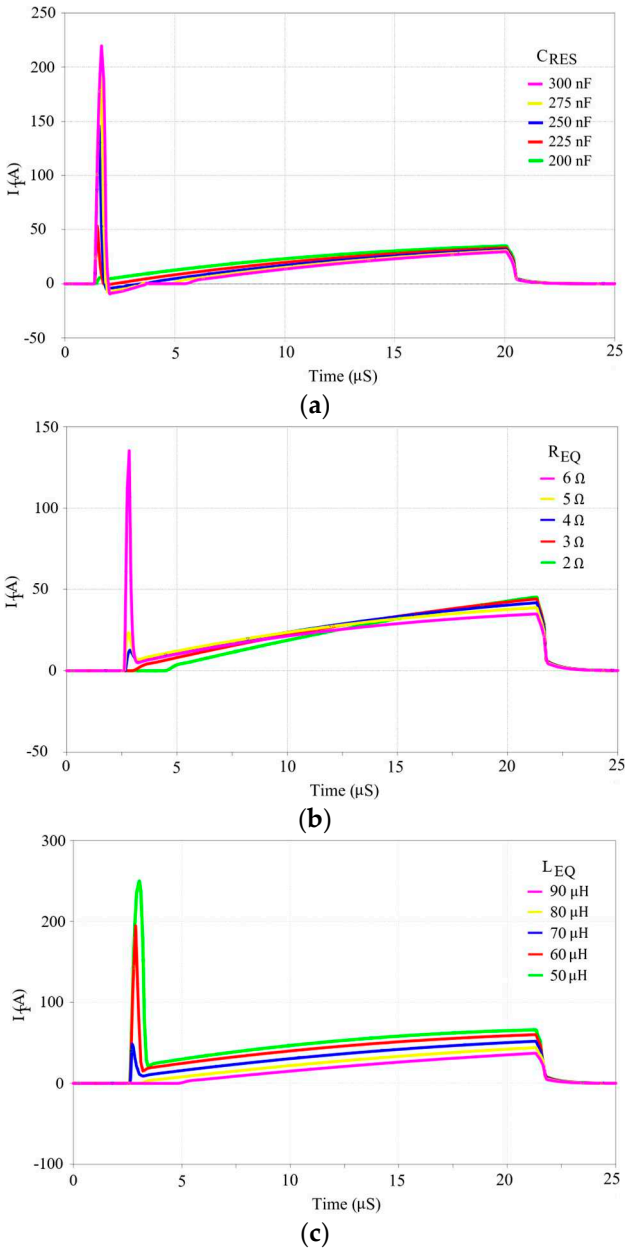

Figure 6. I_T current value variances in PSpice. (a) $R_{EQ} = 3\ \Omega$, $L_{EQ} = 80\ \mu H$ and depending on C_{RES} values. (b) $C_{RES} = 270\ nF$, $L_{EQ} = 80\ \mu H$ and depending on R_{EQ} values. (c) $R_{EQ} = 3\ \Omega$, $C_{RES} = 270\ nF$ depending on L_{EQ} values.

Nonetheless, closed-loop power control techniques and the assessment of input parameters play a pivotal role in ensuring dependable operational conditions. When scrutinizing the quasi-resonant inverter, it becomes evident that its operating modes oscillate between RL and RLC circuits. Consequently, the implementation of closed-loop control methodologies to ascertain the turn-on and turn-off timings of semiconductor switches emerges as indispensable. Depending on the material characteristics, AC supply conditions, and parameters of inverter circuit elements, miscalculations in semiconductor switch turn-on or turn-off times exceeding $1\mu s$ can swiftly escalate switching losses. This outcome can render the switch inoperative due to either overheating or overvoltage occurrences.

In the next section, a new simplified design method for SSQR inverter used in household appliances is examined.

Preprints (www.preprints.org) | NOT PEER-REVIEWED | Posted: 29 August 2023 doi:10.20944/preprints202308.1905.v1

3. Proposed Design Method For Quasi Resonant Inverter

Before starting the inverter design, the circuit variables that we use as input variables and known before the design should be defined correctly and the related design should be guided by using known circuit variables. In this study, the dc source voltage V_{DC} that obtained as a result of rectified of ac mains voltage, the average input power P_{AVG} drawn from the main source, the semiconductor switch turns on time T_{ON} and turn off time T_{OFF} variables are used as the initial conditions. The method to be followed in the design can be summarized as follows:

- The dc source voltage V_{DC}, the average input power P_{AVG}, the switch turns on time T_{ON} and the switch turn off time T_{OFF} variables are defined.
- The maximum value of the coil current I_{LEQMAX} is calculated with the help of the relevant circuit equations.
- By detecting the 1st harmonic component of the voltage applied to the resonant circuit, the load resistance R_{LEQ} is calculated.
- After calculating the load resistance R_{LEQ}, the equivalent inductance value L_{EQ} is calculated with the help of the RL circuit equations.
- It is determined the α, ω_0 and ω_d of the series RLC circuit with the help of calculated variables.
- The resonant capacitor value C_{RES} is calculated with the help of resonant frequency ω_0 and inductance value L_{EQ}.
- The design is verified by calculating the coil current and capacitor voltage boundary conditions.

3.1. Defining of the Time Intervals T_{ON} and T_{OFF}, the Source Voltage V_{DC} and the Input Power P_{AVG}:

In order not to operate at the audible frequency value, the operating frequency values of household induction hobs are not preferred below the $\mathbf{20kHz}$ threshold frequency value [48–50]. On the other hand, to increase the switching frequency will increase the switching losses of the used semiconductors [4,48,51].

$$P_{SW} = f_s . E_{off} \tag{16}$$

For these reasons mentioned above, SSQR inverters used in induction cookers are operated in the range of $20 - 40$kHz. It should also be noted that SSQR inverter circuits cannot be operated directly with frequency control as with half-bridge inverters. $\mathbf{T_{OFF}}$ time is determined by controlling the resonance oscillation of the energy transferred to the load during the $\mathbf{T_{ON}}$ time. The predefined values for starting in this design study are $\mathbf{T_{ON} = 15\mu S}$ and $\mathbf{T_{OFF} = 25\mu S}$. The source voltage $\mathbf{V_{DC}}$ is obtained by rectifying the AC mains voltage, as shown in Figure 7.

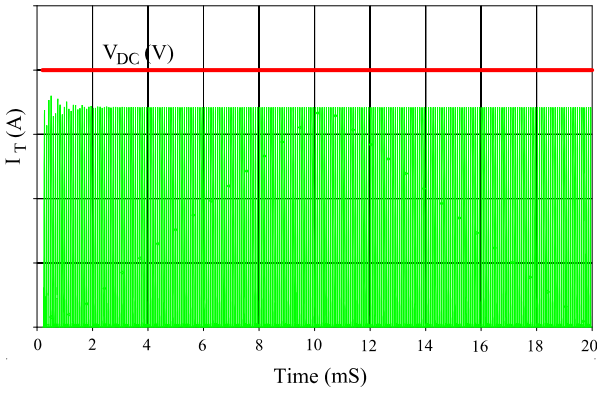

Figure 7. V_{DC} and switch current I_T as a function of time for the case where the source voltage V_{DC} is the DC voltage source.

The purpose of the capacitor used at the output of the rectifier is to provide the instantaneous currents demanded by the inverter circuit and act as a filter. Therefore, the DC voltage obtained follows the form of the main. In order to make the calculations easy and understandable, first of all, $\mathbf{V_{DC}}$ voltage will be accepted as a DC voltage source, and then the calculation values will be updated

Preprints (www.preprints.org) | NOT PEER-REVIEWED | Posted: 29 August 2023 doi:10.20944/preprints202308.1905.v1

for the case where $\mathbf{V_{DC}}$ voltage follows the mains voltage form. The case where the source voltage $\mathbf{V_{DC}}$ is the DC voltage source is shown in Figure 7, and the case where $\mathbf{V_{DC}}$ follows the mains voltage form is shown in Figure 8. Finally, the predefined average source power for this design study is defined as $\mathbf{P_{AVG} = 1250W}$.

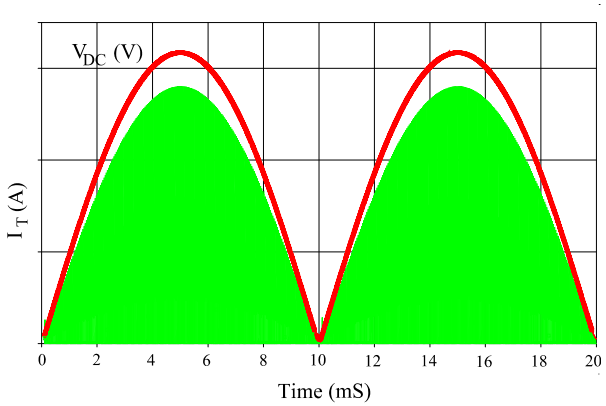

Figure 8. V_{DC} and switch current I_T as a function of time for the case where the source voltage V_{DC} follows the mains voltage form.

3.2. Calculation of the Maximum Coil Current $\boldsymbol{I_{LEQMAX}}$*:*

In the case of quasi resonant inverter circuit operating in **RL** operating mode, the coil current $\mathbf{i_{LEQ}(t)}$ equals the semiconductor switch current $\mathbf{i_T(t)}$ ($i_{LEQ}(t) = i_T(t)$). When the operating states of the quasi-resonant inverter circuit are examined, finding the maximum value of the switch current $\mathbf{i_T(t)}$ means finding the approximate maximum value of the coil current $\mathbf{i_{LEQ}(t)}$.

$$I_{LEQMAX} \approx I_{TMAX} \tag{17}$$

When the source voltage V_{DC} is considered constant as the DC voltage source, the power-time graph becomes the multiplier of the current-time graph. The switch current $\mathbf{i_T(t)}$ and input power $\mathbf{P(t)}$ graphs as a function of time $\mathbf{t}$ are shown in Figures 9 and 10 respectively. The variation of RL circuit switch current $i_T(t)$ with time t depends on the values of R and L and is defined by equation (18) in case $i_{LEQ}(0) = 0$.

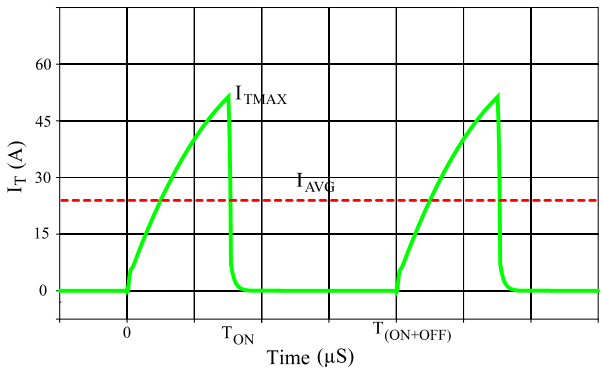

Figure 9. Switch current $i_T(t)$ as a function of time t.

Preprints (www.preprints.org) | NOT PEER-REVIEWED | Posted: 29 August 2023 doi:10.20944/preprints202308.1905.v1

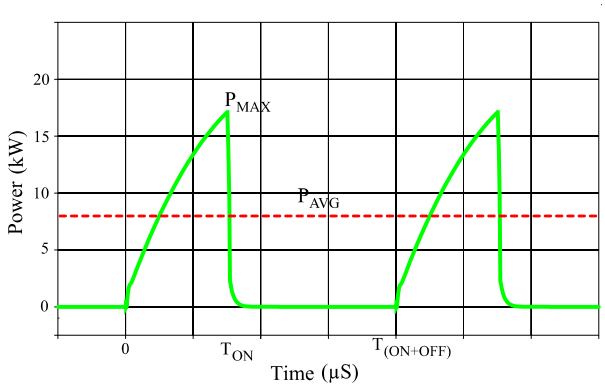

Figure 10. Input power P(t) as a function of time t.

$$i_{LEQ}(t) = i_T(t) = \frac{V_{DC}}{R_{LEQ}} \cdot (1 - e^{-\frac{R_{EQ}}{L_{EQ}}.t}) \tag{18}$$

From equation (18) it is clear that the graphs of $i(t) - t$ and $P(t) - t$ cannot be linear and will behave variably depending on the RL circuit values. However, since the resistance values created by the pots used in induction heated cookers in the primary circuits are in the range of $1\Omega - 5\Omega$, accepting these graphs as linear will be very useful for finding the I_{TMAX} current. For the case where the average power transferred to the RL circuit is defined as P_{AVG} and the instantaneous maximum power is defined as P_{MAX}, the following equation is obtained with the help of Figure 10.

$$P_{AVG} = \frac{P_{MAX}.T_{ON}}{2.(T_{ON} + T_{OFF})} = \frac{V_{DC}.I_{TMAX}.T_{ON}}{2.(T_{ON} + T_{OFF})} \tag{19}$$

As a result of equation (19), I_{TMAX} value can be easily calculated (20).

$$I_{TMAX} = \frac{P_{AVG}.2.(T_{ON} + T_{OFF})}{V_{DC}.T_{ON}} = \frac{P_{MAX}}{V_{DC}} \tag{20}$$

On the other hand, for the case where the source voltage $\mathbf{V_{DC}}$ follows the mains voltage form, let's define the switch current and power variables as shown below:

$I_{TMAX} \rightarrow I_{TMAX2}$
$P_{MAX} \rightarrow P_{MAX2}$
$P_{AVG} \rightarrow P_{AVG2}$
$V_{DC} \rightarrow V_{DC2}$

Equation (21) is written for the case where the average power drawn from the source during the $\pi/2$ interval is accepted as P_{AVG2}, and the average power drawn from the source only at the time of $\pi/2$ is accepted as $P_{AVG2-MAX}$.

$$P_{AVG2} = \frac{1}{\pi}\int_0^{\pi} P_{AVG2-MAX}.\sin\omega t\, d(\omega t) \tag{21}$$

And then the equation (21) is simplified, equation (22) is obtained.

$$P_{AVG2} = P_{AVG2-MAX}.\frac{2}{\pi} \tag{22}$$

When the equations (19) and (20) are rearranged,

$$P_{AVG2-MAX} = \frac{P_{MAX2}.T_{ON}}{2.(T_{ON} + T_{OFF})} = \frac{V_{DC2}.I_{TMAX2}.T_{ON}}{2.(T_{ON} + T_{OFF})} \tag{23}$$

$$I_{TMAX2} = \frac{P_{AVG}.2.(T_{ON} + T_{OFF})}{V_{DC2}.T_{ON}}.\frac{\pi}{2} \tag{24}$$

As can be easily seen from the equations (23) and (24), the switch current I_{TMAX2} and the instantaneous maximum power value P_{MAX2} to be obtained for the case where the source voltage

Preprints (www.preprints.org) | NOT PEER-REVIEWED | Posted: 29 August 2023 doi:10.20944/preprints202308.1905.v1

follows the mains voltage will increase by $\pi/2$ compared to the case where the source voltage is DC. This is because the same P_{AVG} value is desired to be drawn from the source, regardless of the source voltage form.

3.3. Calculation of $\boldsymbol{R_{LEQ}}$ *Value by Determining the 1st Harmonic Component of The DC Voltage:*

Assuming that the resonant circuit current $\mathbf{i_{LEQ}(t)}$ is sinusoidal, the 1st harmonic component of the voltage applied to the resonant circuit is obtained. In this way, the value of resistance **R** is reached by using the maximum value of the resonant circuit current. According to the Fourier theorem, any practical periodic function with an angular frequency of $\boldsymbol{\omega_0}$ can be expressed as an infinite sum of sine or cosine functions that are integer multiples of $\boldsymbol{\omega_0}$ [52]. Thus, $\mathbf{f(t)}$ can be expressed as:

$$f(t) = a_0 + a_1 \cos \omega_0 t + b_1 \sin \omega_0 t \tag{25}$$

The value a_0 is the mean value of the function f(t) and is indicated by the below equation.

$$a_0 = \frac{1}{T}\int_0^T f(t)\, dt \tag{26}$$

The variation of V_{DC} voltage applied to the quasi-resonant circuit as a function of time is shown in Figure 11. The value of a_0 is found with the help of equation (26) so that the $T_{ON} + T_{OFF}$ value is the period of the function.

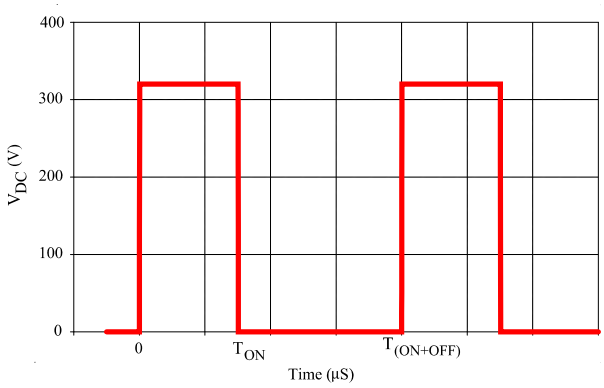

Figure 11. Input voltage V_{DC} as a function of time t.

$$\boldsymbol{a_0} = \frac{1}{T}\int_0^T f(t)\, dt = \frac{1}{T}\int_0^{T_{ON}} V_{DC}\, dt = \boldsymbol{\frac{V_{DC}.T_{ON}}{T_{ON}+T_{OFF}}}$$

And then, a_1 and b_1 values of the related V_{DC} voltage waveform will be found respectively.

$$a_1 = \frac{2}{T}\int_0^T f(t) \cos \omega_0 t\, dt \tag{27}$$

$$a_1 = \frac{2}{T}\int_0^T f(t) \cos \omega_0 t\, dt = \frac{2}{T}\int_0^{T_{ON}} V_{DC} \cos \omega_0 t\, dt$$

$$\boldsymbol{a_1} = \frac{2V_{DC}}{T\omega_0}|\sin \omega_0 t|_0^{T_{ON}} = \boldsymbol{\frac{V_{DC}}{\pi}\sin(\frac{2\pi.T_{ON}}{T_{ON}+T_{OFF}})}$$

$$b_1 = \frac{2}{T}\int_0^T f(t) \sin \omega_0 t\, dt \tag{28}$$

$$b_1 = \frac{2}{T}\int_0^T f(t) \sin \omega_0 t\, dt = \frac{2}{T}\int_0^{T_{ON}} V_{DC} \sin \omega_0 t\, dt$$

Preprints (www.preprints.org) | NOT PEER-REVIEWED | Posted: 29 August 2023 doi:10.20944/preprints202308.1905.v1

$$\boldsymbol{b_1} = \frac{2V_{DC}}{T\omega_0}|-cos\,\omega_0 t|_0^{T_{ON}} = \frac{\boldsymbol{V_{DC}}}{\boldsymbol{\pi}}\left(\boldsymbol{1} - \boldsymbol{cos}\left(\frac{\boldsymbol{2\pi.T_{ON}}}{\boldsymbol{T_{ON}+T_{OFF}}}\right)\right)$$

It is also possible to represent the equation in (25) in amplitude-phasor form [52].

$$f(t) = a_0 + A_1\cos(\omega_0 t + \phi) \tag{29}$$

$$A_1 = \sqrt{a_1^2 + b_1^2} \tag{30}$$

In (30) A_1 is the amplitude value of the 1st harmonic component of the f(t) function. And so, the next steps are to find the amplitude, in other words, the peak value of the 1st harmonic component of the V_{DC} voltage applied to the quasi-resonant circuit, and to reach the R_{EQ} value by proportioning this value to the maximum value of the coil current I_{LEQMAX}.

$$A_1 = \sqrt{\left(\frac{V_{DC}}{\pi}\sin(\frac{2\pi.T_{ON}}{T_{ON}+T_{OFF}})\right)^2 + \left(\frac{V_{DC}}{\pi}(1-\cos\left(\frac{2\pi.T_{ON}}{T_{ON}+T_{OFF}}\right))\right)^2}$$

$$i_{LEQMAX} \approx I_{TMAX} = \frac{P_{AVG}.2.(T_{ON}+T_{OFF})}{V_{DC}.T_{ON}}$$

$$\boldsymbol{R_{EQ}} = \frac{\boldsymbol{A_1}}{\boldsymbol{i_{LEQMAX}}} \tag{31}$$

3.4. Calculation of the Equivalent Inductance Value $\boldsymbol{L_{EQ}}$*:*

In order to calculate the $\mathbf{L_{EQ}}$ inductance value, 3 different methods are used, and the results are compared with each other and verified. The first of these is to use the current equation of the series RL circuit, the second is to use the voltage at the inductor ends, and the third is to calculate the inductance value by using the energy accumulated in the inductor.

3.4.1. L_{EQ} calculation using series RL circuit switch current i_T value:

As mentioned earlier, the series RL circuit switch current $i_T(t)$ as a function of time t, depends on the R_{EQ} and L_{EQ} values and is defined by equation (32) for $i_{LEQ}(0) = 0$.

$$i_{LEQ}(t) = i_T(t) = \frac{V_{DC}}{R_{LEQ}} \cdot (1 - e^{-\frac{R_{EQ}}{L_{EQ}}.t}) \tag{32}$$

Since the source voltage V_{DC}, equivalent resistance R_{EQ}, maximum value of coil current I_{LEQMAX} and time information T_{ON} are now known, $\mathbf{L_{EQ}}$ value can be found by using equation (33).

$$\boldsymbol{L_{EQ}} = -\frac{R_{LEQ}.T_{ON}}{Ln\left(1 - \frac{R_{LEQ}.I_{LEQMax}}{V_{DC}}\right)} \tag{33}$$

3.4.2. L_{EQ} calculation using inductor voltage V_{LEQ} value:

Equation (34) is obtained by using Kirchhoff's voltage law in series RL circuit.

$$V_{DC} = V_{LEQ} + V_{REQ} \tag{34}$$

And also, the voltage V_{LEQ} at the inductor ends is presented by the below equation (35).

$$v_{LEQ} = L_{EQ}\frac{di_{LEQ}(t)}{dt} \tag{35}$$

We will also make the linearity assumption that we used when finding the I_{TMAX} current in the series RL circuit. The inductance value for this range where the semiconductor switch and coil currents are equal to each other indicated by the below equation.

Preprints (www.preprints.org) | NOT PEER-REVIEWED | Posted: 29 August 2023 doi:10.20944/preprints202308.1905.v1

$$L_{EQ} = V_{LEQ}.\frac{\Delta t}{\Delta i_{LEQ}} = (V_{DC} - V_{REQ})\frac{T_{ON}}{I_{TMAX}} \quad (36)$$

Although the V_{DC} voltage is constant, the V_{REQ} voltage is expressed as (37) for the case where the current is considered linear.

$$V_{REQ} = \frac{I_{TMAX}.R_{EQ}}{2} \quad (37)$$

When this expression is substituted in (36), the equation (38) is reached.

$$\boldsymbol{L_{EQ}} = (V_{DC} - \frac{I_{TMAX}.R_{EQ}}{2})\frac{T_{ON}}{I_{TMAX}} \quad (38)$$

3.4.3. L_{EQ} calculation using inductor energy W_{LEQ} value:

The energy accumulated in the inductor is expressed by the equation (39) in terms of inductance and inductor current.

$$W_{LEQMAX} = \frac{1}{2}L_{EQ}.{I_{LEQMAX}}^2 \quad (39)$$

When the area under the $P(t) - t$ graph shown in Figure 10 is integrated, the total energy transferred to the series RL circuit is found. Assuming the $P(t) - t$ graph as linear (40) is found.

$$W_{MAX} = \frac{P_{MAX}.T_{ON}}{2} \quad (40)$$

To find the total energy transferred to the inductor, the energy dissipated in the resistor is subtracted from the total energy transferred to the series RL circuit.

$$W_{LEQMAX} = W_{MAX} - W_{REQMAX} \quad (41)$$

Equation (42) is obtained as a result of equations (40) and (41).

$$W_{LEQMAX} = \frac{P_{MAX}.T_{ON}}{2} - \left(\frac{I_{TMAX}}{2}\right)^2.R_{EQ} \quad (42)$$

After the energy accumulated in the inductor is reached, equation (43) is used to arrive at the L_{EQ} equivalent inductance.

$$\frac{1}{2}L_{EQ}.{I_{LEQMAX}}^2 = \frac{P_{MAX}.T_{ON}}{2} - \left(\frac{I_{TMAX}}{2}\right)^2.R_{EQ} \quad (43)$$

And finally, it is getting the equation (44) by the help of equations (39) and (43).

$$\boldsymbol{L_{EQ}} = \frac{2}{{I_{TMAX}}^2}\left(\frac{P_{MAX}.T_{ON}}{2} - \left(\frac{I_{TMAX}}{2}\right)^2.R_{EQ}\right) \quad (44)$$

3.5. Determination The Series RLC Circuit Parameters:

Since the $\mathbf{T_{OFF}}$ time, which is the turnoff time of the semiconductor switch, is defined and known before the design, and the $\mathbf{L_{EQ}}$ and $\mathbf{R_{EQ}}$ values are calculated, the damping coefficient $\boldsymbol{\alpha}$, resonant frequency $\boldsymbol{\omega_0}$ and damped resonant frequent $\boldsymbol{\omega_d}$ values of the series **RLC** circuit can be calculated easily. First, the damped resonant frequency $\boldsymbol{\omega_d}$ is calculated by using the relationship between the $\mathbf{T_{OFF}}$ time and the resonant frequency $\mathbf{T_{RES}}$ of the series **RLC** circuit.

$$T_{RES} \approx T_{OFF}.\frac{4}{3} \quad (45)$$

$$f_{RES} = f_d = \frac{1}{T_{RES}} \quad (46)$$

Preprints (www.preprints.org) | NOT PEER-REVIEWED | Posted: 29 August 2023 doi:10.20944/preprints202308.1905.v1

$$\omega_d = 2\pi f_d = \frac{2\pi}{T_{RES}} \tag{47}$$

$$\boldsymbol{\omega_d} = \frac{2\pi}{T_{OFF}}.\frac{3}{4} \tag{48}$$

And then, the damping coefficient α of the series RLC circuit is found by the equation (49).

$$\boldsymbol{\alpha} = \frac{R_{EQ}}{2L_{EQ}} \tag{49}$$

Finally, the resonant frequency ω_0 is calculated with the help of the equation (51).

$$\omega_d = \sqrt{\omega_0{}^2 - \alpha^2} \tag{50}$$

$$\boldsymbol{\omega_0} = \sqrt{\omega_d{}^2 + \alpha^2} \tag{51}$$

3.6. Calculation of the Resonant Circuit Capacitor Value Inductance Value $\boldsymbol{C_{RES}}$*:*

After calculating the resonant frequency $\boldsymbol{\omega_0}$ and the equivalent inductance $\mathbf{L_{EQ}}$ values, the resonant circuit capacitance value $\mathbf{C_{RES}}$ is found by using equation (52).

$$\boldsymbol{\omega_0} = \frac{\mathbf{1}}{\sqrt{\boldsymbol{L_{EQ}C_{RES}}}} \tag{52}$$

$$\boldsymbol{C_{RES}} = \frac{\mathbf{1}}{\boldsymbol{L_{EQ}}(\boldsymbol{\omega_0})^{\mathbf{2}}} \tag{53}$$

3.7. Calculation of Current and Voltage Boundary Conditions of Semiconductor Switch:

Defining boundary conditions for the single switch inverter design is very important. In working stage II and stage III (series **RLC** circuit mode) the coil current $\mathbf{I_{LEQ}}$ and switch voltage $\mathbf{V_{CE}}$ values reach their maximum values. Knowledge about these two parameters is very important and valuable for the designer not only for reliable working conditions but also to control system parameters such as power. As it can be seen from Figure 3 that when the coil current $\mathbf{I_{LEQ}}$ reach its maximum value $\mathbf{I_{LEQMAX}}$, the derivation of the $\mathbf{I_{LEQ}}$ current is zero ($\mathbf{t = t_1}$). As result of this the maximum coil current $\mathbf{I_{LEQMAX}}$ can be derived by the help of (54)-(56).

$$di_{LEQ}(t_1)/dt = 0 \implies i_{LEQ}(t_1) = I_{LEQMAX} \tag{54}$$

$$t_1 = tan^{-1}[-(B_1\alpha - B_2\omega_d)/(B_1\omega_d + B_2\alpha)])/\omega_d \tag{55}$$

$$\boldsymbol{I_{LEQMAX}} = i_{LEQ}(t_1) = e^{-\alpha t_1}(B_1 cos(\omega_d t_1) + B_2 sin(\omega_d t_1)) \tag{56}$$

Single switch induction cooker's maximum power level is limited by power switch maximum breakdown voltage level. When the switch voltage V_{CE} reach its maximum value V_{CEMAX}, the I_{LEQ} current is zero ($t = t_3$). As result of this the maximum switch voltage V_{CEMAX} can be derived by the help of (57)-(59).

$$i_{LEQ}(t_3) = 0 \implies v(t_3) = V_{CEMAX} \tag{57}$$

$$t_3 = tan^{-1}(-B_1/B_2)/\omega_d \tag{58}$$

$$\boldsymbol{V_{CEMAX}} = v(t_3) = V_{DC} + e^{-\alpha t_3}(A_1 cos(\omega_d t_3) + A_2 sin(\omega_d t_3)) \tag{59}$$

Preprints (www.preprints.org) | NOT PEER-REVIEWED | Posted: 29 August 2023 doi:10.20944/preprints202308.1905.v1

3.8. The Flowchart of the Proposed Design Method

The flowchart shown in Figure 12 is developed to understand the determining of the L_{EQ} and R_{EQ} more clearly. It determines the boundary conditions of the semiconductor switch with the help of the same flow chart. If the boundary conditions are not within the defined safe limit values of the semiconductor, the design is started from the beginning.

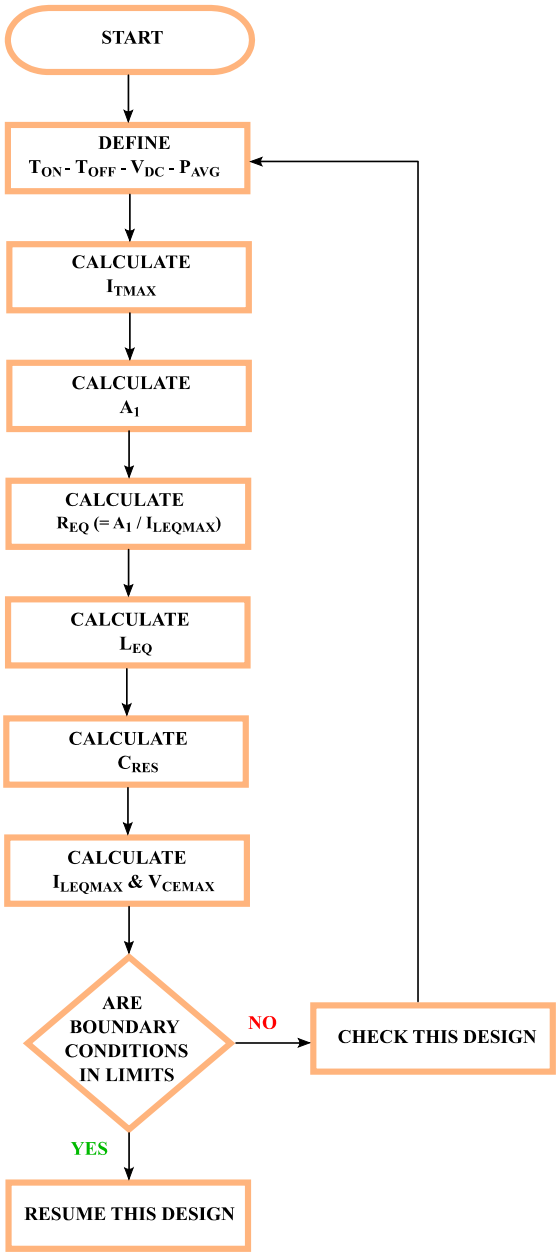

Figure 12. Flowchart of proposed method to determine L_{EQ}, R_{EQ}, I_{LEQMAX} and V_{CEMAX}.

4. Verification of Proposed Analysis Method

In order to prove the accuracy of the proposed design method, first of all, critical circuit parameter values are calculated using predefined input parameters depending on the design requirements. By using the circuit parameters obtained as a result of the calculation, simulation studies are carried out and the boundary conditions required to ensure reliable operation of the inverter circuit are measured.

Preprints (www.preprints.org) | NOT PEER-REVIEWED | Posted: 29 August 2023 doi:10.20944/preprints202308.1905.v1

4.1. Calculation Results

As a result of the proposed method and calculation tools, a standard design example has been carried out and the calculated results are listed in Table 1. Firstly, the initial values are defined and then the critical circuit elements' values are calculated. As previously mentioned, the average source power for this design study is defined as the $\mathbf{P_{AVG} = 1275W}$. And also, the switch turn-on and turn-off times are defined as the $\mathbf{T_{ON} = 15\mu S}$ and $\mathbf{T_{OFF} = 25\mu S}$. The source voltage $\mathbf{V_{DC}}$ is obtained by rectifying the $\mathbf{AC}$ mains voltage.

Table 1. Calculating circuit parameters.

Pre-Defined Circuit Parameters	
T_{ON}	**15 µS**
T_{OFF}	**25 µS**
P_{AVG}	**1275 W**
V_{AC}	**230 VAC**
V_{DC2}	**325, 27 VDC**
Calculated Circuit Parameters	
P_{AVG2}	**1275 W**
$P_{AVG2-MAX}$	**2002, 77 W**
P_{MAX2}	**10681, 42W**
I_{TMAX2}	**32 , 84A**
a_0	**121, 97**
a_1	**73, 21**
b_1	**176, 75**
A_1	**191, 31**
R_{EQ}	**5, 83 Ω**
L_{EQ}	**98, 5 µH**
T_{RES}	**33, 33 µS**
f_{RES}	**30 kHz**
ω_d	**188495, 56**
α	**29570, 68**
ω_0	**190800, 95**
C_{RES}	**278, 86 nF**
Calculated Boundary Conditions	
I_{LEQMAX}	**33, 57 *A***
V_{CEMAX}	**834, 49 *V***

The critical circuit elements values are calculated as $\mathbf{R_{EQ} = 5,83\Omega}$, $\mathbf{L_{EQ} = 98,5\mu H}$, and $\mathbf{C_{RES} = 278,86nF}$. In addition to circuit parameters $\mathbf{L_{EQ}}$ and $\mathbf{R_{EQ}}$, the current and voltage boundary conditions of the semiconductor switch are calculated to check design reliability. As can be seen from Table 1, depending on the input values defined for this study, the maximum value of the switch voltage $\mathbf{V_{CEMAX}}$ is calculated as $\mathbf{834,49V}$, and the maximum value of the switch current $\mathbf{I_{LEQMAX}}$ is calculated as $\mathbf{33,57A}$.

4.2. Simulation Results

A simulation prototype circuit has been developed using the predefined and calculated circuit parameters from Table 1, and it is shown in Figure 13. The OrCAD PSpice software program has been used for the simulation, with a particular emphasis on ensuring that the maximum coil current ($\mathbf{I_{LEQMAX}}$) and maximum switch voltage ($\mathbf{V_{CEMAX}}$) values align with the values calculated in the previous section.

Preprints (www.preprints.org) | NOT PEER-REVIEWED | Posted: 29 August 2023 doi:10.20944/preprints202308.1905.v1

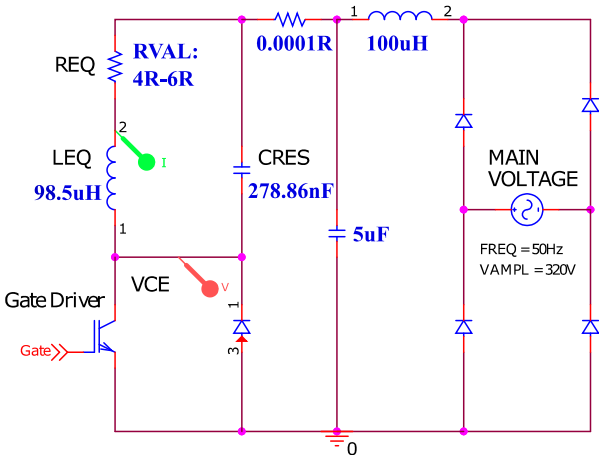

Figure 13. Prototype simulation circuit for proposed converter.

When the critical circuit element values obtained from measurement results were directly used in the designed circuit for simulation, some deviations were observed in the $\mathbf{I_{LEQMAX}}$ and $\mathbf{V_{CEMAX}}$ values. The measured switch voltage was found to be $\mathbf{760V}$ instead of the expected $\mathbf{835V}$, resulting in an error of approximately $\mathbf{9}\%$. Similarly, the maximum coil current, which should have been $\mathbf{33.57A}$, was measured as $\mathbf{30.85A}$, indicating an error of approximately $\mathbf{8}\%$.

Although the deviation values might be acceptable for many designers, the root cause of the discrepancy has been investigated to continue the simulation studies. It was hypothesized that the deviation arose from the proposed design method, which assumed a linear current-time graph by neglecting the resistance value in the RL operating mode of the SSQR inverter. Based on this assumption, a sweep analysis method has been employed in the relevant simulation program, scanning $\mathbf{R_{EQ}}$ resistance values between $4\mathbf{\Omega}$ and $6\mathbf{\Omega}$ with a precision of $0{,}1\mathbf{\Omega}$. The resistance value that yielded the same current and voltage values as the calculated ones has been determined. Figure 14 illustrates the graph of the obtained current and voltage values from the scanning process. It has been observed that when a resistance value of $4{,}3\mathbf{\Omega}$ was used instead of the calculated resistance value of $5{,}83\mathbf{\Omega}$, the calculated values matched exactly with the simulation results. All the results obtained from the scanning process are presented numerically in Table 2.

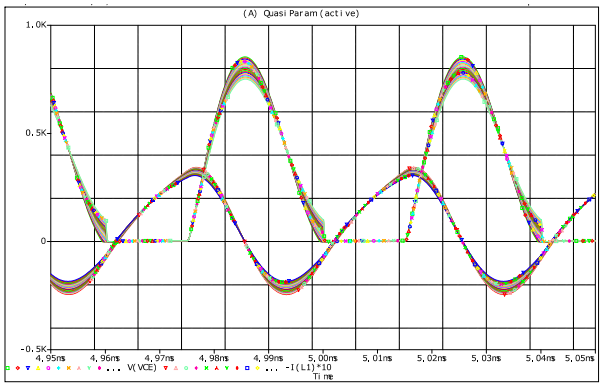

Figure 14. Coil current I_{LEQ} and switch voltage V_{CE} for sweeped R_{EQ} values as a function of time t.

Table 2. Simulation circuit results.

Input Circuit Parameters		Output Boundary Parameters		Output Power	
R_{EQ}	L_{EQ}	C_{RES}	I_{LEQMAX}	V_{CEMAX}	P_{AVG2}
4,0 Ω	98,5 μH	278,86 nF	34,20 A	852 V	1060 W
4,1 Ω	98,5 μH	278,86 nF	34,00 A	846 V	1080 W
4,2 Ω	98,5 μH	278,86 nF	33,80 A	842 V	1100 W
4,3 Ω	**98,5 μH**	**278,86 nF**	**33,60 A**	**835 V**	**1110 W**

Preprints (www.preprints.org) | NOT PEER-REVIEWED | Posted: 29 August 2023 doi:10.20944/preprints202308.1905.v1

4,4 Ω	98,5 μH	278,86 nF	33,40 A	832 V	1120 W
4,5 Ω	98,5 μH	278,86 nF	33,30 A	826 V	1130 W
4,6 Ω	98,5 μH	278,86 nF	33,10 A	821 V	1140 W
4,7 Ω	98,5 μH	278,86 nF	32,90 A	815 V	1150 W
4,8 Ω	98,5 μH	278,86 nF	32,70 A	810 V	1155 W
4,9 Ω	98,5 μH	278,86 nF	32,50 A	805 V	1160 W
5,0 Ω	98,5 μH	278,86 nF	32,30 A	800 V	1165 W
5,1 Ω	98,5 μH	278,86 nF	32,10 A	795 V	1170 W
5,2 Ω	98,5 μH	278,86 nF	31,90 A	790 V	1180 W
5,3 Ω	98,5 μH	278,86 nF	31,75 A	785 V	1190 W
5,4 Ω	98,5 μH	278,86 nF	31,60 A	780 V	1200 W
5,5 Ω	98,5 μH	278,86 nF	31,45 A	775 V	1210 W
5,6 Ω	98,5 μH	278,86 nF	31,20 A	770 V	1215 W
5,7 Ω	98,5 μH	278,86 nF	31,05 A	765 V	1220 W
5,8 Ω	**98,5 μH**	**278,86 nF**	**30,85 A**	**760 V**	**1225 W**
5,9 Ω	98,5 μH	278,86 nF	30,70 A	755 V	1230 W
6,0 Ω	98,5 μH	278,86 nF	30,50 A	750 V	1235 W

To compare the results from the simulation circuit with the application circuit under the same conditions, the coil current ($\mathbf{I_{LEQ}}$) and switch voltage ($\mathbf{V_{CE}}$) graphs are separately presented over a 20ms time interval in Figures 15 and 16. The primary advantage of this representation is to provide a comprehensive and detailed understanding of how these variables change over time for those examining the study. By placing the simulation and application circuit results side by side, researchers can directly compare them and assess the accuracy or deviation between the simulated and actual circuit performance. This comparative analysis allows for a better understanding of the similarities and differences, enabling researchers to gain insights into potential factors that may affect the circuit's behavior. Furthermore, by examining the variation of coil current and switch voltage over time, researchers can gain valuable insights into the dynamic behavior of the circuit. This information can be used to optimize the circuit's performance, identify potential issues such as transient spikes or oscillations, and make informed design decisions to ensure the circuit operates within desired parameters.

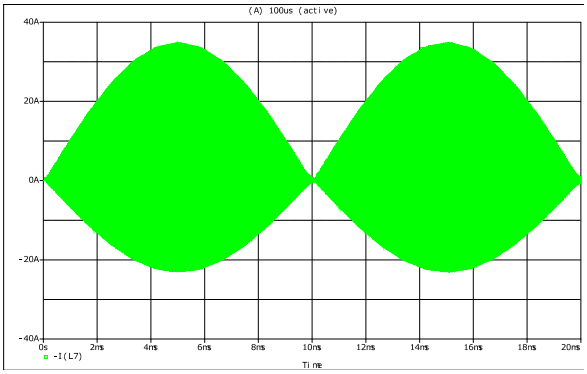

Figure 15. Coil current I_{LEQ} as a function of time t obtained using the simulation circuit.

Preprints (www.preprints.org) | NOT PEER-REVIEWED | Posted: 29 August 2023 doi:10.20944/preprints202308.1905.v1

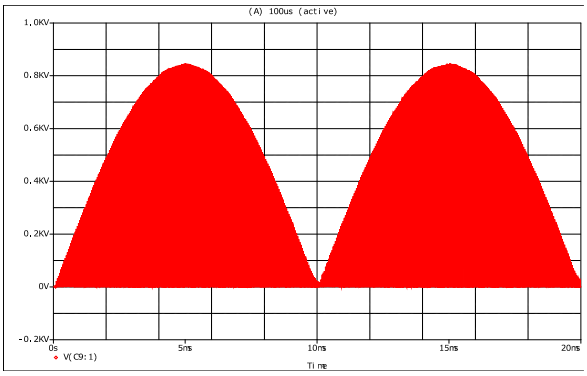

Figure 16. Switch voltage V_{CE} as a function of time t obtained using the simulation circuit.

4.3. Experimental Results

Once the theoretical calculations and simulation studies developed for the calculation of critical circuit parameters are completed, the outputs of the proposed calculation method are tested using a practical application circuit. Before examining the results of the application circuit, it is beneficial to review the technical specifications of the induction coil and the heated pans used in the application circuit. This will facilitate the interpretation of deviations between the practical application results and the theoretical calculations and simulation circuit results.

As described in detail in the introduction of the study, a wide range of pan types are used in household induction cooktops. The electrical effects of these pans on the electronic circuitry are particularly critical due to their ability to change the equivalent resistance and equivalent inductance values. However, it is not feasible to test all possible pan models in practical applications. Therefore, in the experimental implementation of the proposed method, three different pan models with different electrical and magnetic characteristics, as shown in Figure 17, have been used. These pan models include cast iron, stainless steel, and specially designed alloy pans for induction heating.

Figure 17. General pan models are used with induction cookers.

On the other hand, Table 3 provides the physical and electrical characteristics of the induction coil used in the practical application circuit, as well as the measured equivalent inductance and resistance values when using three different types of pans. In practical application, although an exact match of the calculated resistance and inductance values obtained through the proposed calculation method is not achieved, the feasibility of the proposed method has been demonstrated.

Preprints (www.preprints.org) | NOT PEER-REVIEWED | Posted: 29 August 2023 doi:10.20944/preprints202308.1905.v1

Table 3. Technical specifications of the reference induction coil.

Parameter	Symbol	Value	Unit
Number of turns	n	28	
External diameter of the coil	a_n	180	mm
Inner diameter of the coil	a_1	30	mm
Distance between coil winding and ferrite bars	h	4	mm
Distance between coil winding and pan	d	4	mm
Strand amount of a litz wire		66	
Wire diameter of single strand		0,27	mm
Ferrite permeability	μ_r	800	
Equivalent inductance with no load	$L_{EQNoLoad}$	110	µH
Equivalent resistance with no load	$R_{EQNoLoad}$	0,12	Ω
Equivalent inductance with cast iron pan	L_{EQPan}	89,76	µH
Equivalent resistance with cast iron pan	R_{EQPan}	4,21	Ω
Equivalent inductance with stainless steel pan	L_{EQPan}	81,81	µH
Equivalent resistance with stainless steel pan	R_{EQPan}	3,36	Ω
Equivalent inductance with silit silargan pan	L_{EQPan}	69,07	µH
Equivalent resistance with silit silargan pan	R_{EQPan}	2,48	Ω

The coil current, the switch voltage and the output power values obtained when using three different pan models are presented in Table 4. In addition, in Table 5, the output results obtained using the calculation, simulation and application circuit for similar conditions are compared. Upon closer examination of Table 5, it is evident that the values obtained through the calculation method closely match the nearest capacitor value used.

Table 4. Experimental circuit results.

Input Circuit Parameters		Output Boundary Parameters		Output Power	
R_{EQ}	L_{EQ}	C_{RES}	I_{LEQMAX}	V_{CEMAX}	P_{AVG2}
4,21 Ω	89,76 μH	270 nF	42,4 A	928 V	1276 W
3,36 Ω	81,81 μH	270 nF	42,8 A	968 V	1270 W
2,48 Ω	69,07 μH	270 nF	45,6 A	920 V	1255 W

Table 5. Comparison of the calculation, simulation, and experimental circuit results.

Input Circuit Parameters		Output Boundary Parameters		Output Power	
R_{EQ}	L_{EQ}	C_{RES}	I_{LEQMAX}	V_{CEMAX}	P_{AVG2}
Calculation Results					
5,83 Ω	98,5 μH	278,86 nF	33,57 A	834,49 V	1275 W
Simulation Results					
4,3 Ω	98,5 μH	278,86 nF	33,60 A	835 V	1110 W
5,8 Ω	98,5 μH	278,86 nF	30,85 A	760 V	1225 W
Experimental Results					
4,21 Ω	89,76 μH	270 nF	42,4 A	928 V	1276 W
3,36 Ω	81,81 μH	270 nF	42,8 A	968 V	1270 W
2,48 Ω	69,07 μH	270 nF	45,6 A	920 V	1255 W

However, the different electrical characteristics of the pans used in practical applications make it challenging to directly compare the calculation and application circuits. In practical implementation, a coil current ($\mathbf{I_{LEQMAX}}$) of $\mathbf{42,4A}$ and a switch voltage ($\mathbf{V_{CEMAX}}$) of **928V** have been measured for a resistance of $\mathbf{4,21\Omega}$, while in theoretical calculations and simulation circuit, these values were $\mathbf{33,6A}$ and **835V**, respectively. The deviation is approximately **20**% for current and **10**% for voltage. The main reason for this discrepancy is the change in the resistance and

Preprints (www.preprints.org) | NOT PEER-REVIEWED | Posted: 29 August 2023 doi:10.20944/preprints202308.1905.v1

inductance values measured at the initial conditions when the pan is heated. As a result of these studies, considering the variety of pans used in practical applications, the proposed calculation method is proven to be reliable for initiating the design process.

To compare the results from the simulation circuit with the application circuit under the same conditions, the coil current ($\mathbf{I_{LEQ}}$) and switch voltage ($\mathbf{V_{CE}}$) graphs are separately presented over a 20ms time interval in Figures 18 and 19. When comparing these graphs with the results obtained from the simulation circuit in Figures 15 and 16, it is evident that very similar results can be achieved. Also, the detailed waveforms of the coil current and switch voltage are shown in Figure 20. Finally, the experimental setup is shown in Figure 21.

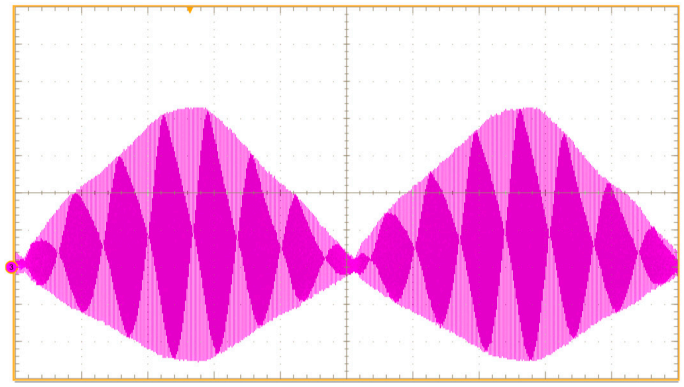

Figure 18. Coil current I_{LEQ} as a function of time t obtained using the prototype circuit.

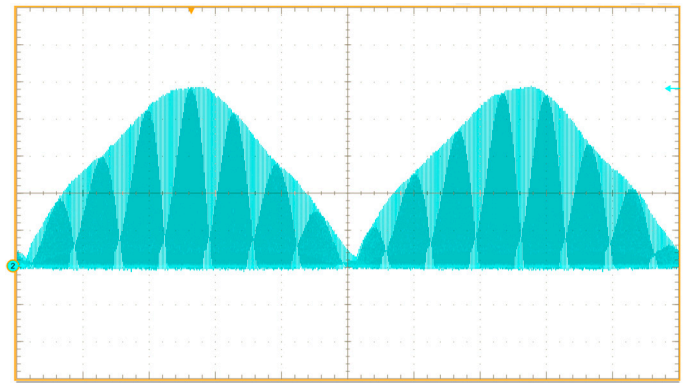

Figure 19. IGBT collector emitter voltage V_{CE} as a function of time t obtained using the prototype circuit.

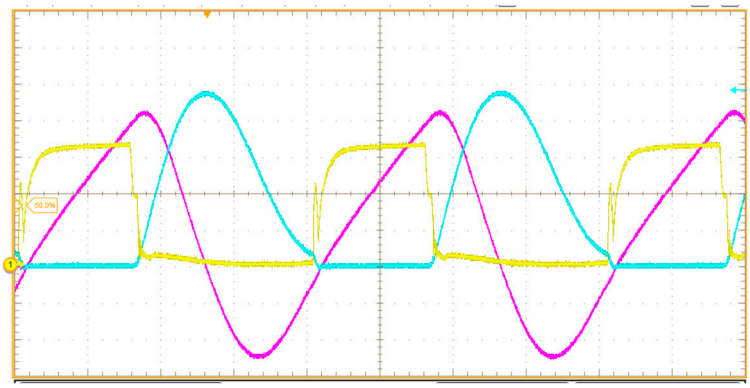

Figure 20. Detailed waveforms obtained using the prototype circuit. Blue signal: IGBT collector emitter voltage V_{CE} (200V/div), Purple signal: coil current I_{LEQ} (10A/div), Yellow signal: IGBT gate control signal (5V/div).

Preprints (www.preprints.org) | NOT PEER-REVIEWED | Posted: 29 August 2023 doi:10.20944/preprints202308.1905.v1

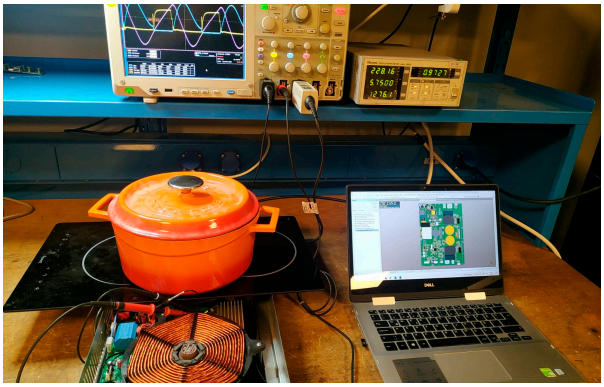

Figure 21. Experimental setup.

5. Conclusions

This paper is focused on a new design method for SSQR inverter used in household appliances. Before starting the inverter design, the circuit variables that we use as input variables and known before the design should be defined correctly and the related design should be guided by using known circuit variables. In this study, the dc source voltage V_{DC} that obtained as a result of rectified of ac mains voltage, the average input power P_{AVG} drawn from the main source, the semiconductor switch turns on time T_{ON} and turn off time T_{OFF} variables are used as the initial conditions. In order to prove the accuracy of the proposed design method, first of all, critical circuit parameter values are calculated using predefined input parameters depending on the design requirements. By using the circuit parameters obtained as a result of the calculation, simulation studies are carried out and the boundary conditions required to ensure reliable operation of the inverter circuit are measured.

After the completion of the theoretical background and simulation studies developed for use in critical circuit parameter calculation studies, the outputs of the relevant design method are run with the help of a practical application circuit. The results obtained from the experimental circuit are also compatible with the simulation results. The reliability of the proposed design and calculation method is proven by comparing the data obtained as a result of the simulation and experimental with the data obtained as a result of the calculation.

Author Contributions: Conceptualization, M.O.; methodology, M.O.; validation, M.O.; investigation, M.O.; writing—original draft preparation, M.O.; writing—review and editing, M.O. All authors have read and agreed to the published version of the manuscript.

Funding: This research received no external funding.

Data Availability Statement: No new data were created.

Acknowledgments: This work was supported by the Scientific and Technological Research Council of Turkey and co-financed by the Mamur Technology Systems Research and Development Center under Project 3210188.

Conflicts of Interest: The authors declare no conflict of interest.

References

1. W. P. W. KOMATSU, "A simple and reliable class E inverter for induction heating applications," *Int. J. Electron.*, vol. 84, no. 2, pp. 157–165, Feb. 1998, doi: 10.1080/002072198134922.
2. H. OMORI and M. NAKAOKA, "New single-ended resonant inverter circuit and system for induction-heating cooking apparatus," *Int. J. Electron.*, vol. 67, no. 2, pp. 277–296, Aug. 1989, doi: 10.1080/00207218908921081.
3. T. Tanaka, "A new induction cooking range for heating any kind of metal vessels," *IEEE Trans. Consum. Electron.*, vol. 35, no. 3, pp. 635–641, 1989, doi: 10.1109/30.44329.
4. O. Lucía, P. Maussion, E. Dede, and J. M. Burdío, "Induction heating technology and its applications: Past Developments, current Technology, and future challenges," *IEEE Trans. Ind. Electron.*, vol. 61, no. 05, pp. 2509–2520, 2014, doi: 10.1109/TIE.2013.2281162.

5. O. Lucia, D. Navarro, P. Guillen, H. Sarnago, and S. Lucia, "Deep Learning-Based Magnetic Coupling Detection for Advanced Induction Heating Appliances," *IEEE Access*, vol. 7. pp. 181668–181677, 2019, doi: 10.1109/ACCESS.2019.2960109.
6. U. Has and D. Wassilew, "Temperature control for food in pots on cooking hobs," *IEEE Trans. Ind. Electron.*, vol. 46, no. 5, pp. 1030–1034, 1999, doi: 10.1109/41.793352.
7. C. Ekkaravarodome, P. Charoenwiangnuea, and K. Jirasereeamornkul, "The simple temperature control for induction cooker based on class-E resonant inverter," in *2013 10th International Conference on Electrical Engineering/Electronics, Computer, Telecommunications and Information Technology*, May 2013, pp. 1–6, doi: 10.1109/ECTICon.2013.6559634.
8. M. K. Kazimierczuk and S. Wang, "Frequency-domain analysis of series resonant converter for continuous conduction mode," *IEEE Trans. Power Electron.*, vol. 7, no. 2, pp. 270–279, Apr. 1992, doi: 10.1109/63.136243.
9. O. Lucia, H. Sarnago, and J. M. Burdio, "Soft-stop optimal trajectory control for improved operation of the series resonant multi-inverter," *IECON Proc. (Industrial Electron. Conf.*, pp. 3283–3288, 2014, doi: 10.1109/IECON.2014.7048982.
10. D. Paesa, C. Franco, S. Llorente, G. Lopez-Nicolas, and C. Sagues, "Adaptive Simmering Control for Domestic Induction Cookers," *IEEE Trans. Ind. Appl.*, vol. 47, no. 5, pp. 2257–2267, Sep. 2011, doi: 10.1109/TIA.2011.2161629.
11. M. Ozturk, F. Zungor, B. Emre, and B. Oz, "Quasi Resonant Inverter Load Recognition Method," *IEEE Access*, vol. 10, no. August, pp. 89376–89386, 2022, doi: 10.1109/ACCESS.2022.3201355.
12. V. Crisafulli and C. V. Pastore, "New control method to increase power regulation in a AC/AC quasi resonant converter for high efficiency induction cooker," in *Proceedings - 2012 3rd IEEE International Symposium on Power Electronics for Distributed Generation Systems, PEDG 2012*, 2012, pp. 628–635, doi: 10.1109/PEDG.2012.6254068.
13. H. Sarnago, O. Lucia, A. Mediano, and J. M. Burdio, "A Class-E Direct AC–AC Converter With Multicycle Modulation for Induction Heating Systems," *IEEE Trans. Ind. Electron.*, vol. 61, no. 5, pp. 2521–2530, May 2014, doi: 10.1109/TIE.2013.2281164.
14. H. Sarnago, O. Lucia, A. Mediano, and J. M. Burdio, "Direct AC–AC Resonant Boost Converter for Efficient Domestic Induction Heating Applications," *IEEE Trans. Power Electron.*, vol. 29, no. 3, pp. 1128–1139, Mar. 2014, doi: 10.1109/TPEL.2013.2262154.
15. P. Vishnuram and G. Ramachandiran, "Capacitor-less induction heating system with self-resonant bifilar coil," *International Journal of Circuit Theory and Applications*, vol. 48, no. 9. pp. 1411–1425, 2020, doi: 10.1002/cta.2830.
16. H. P. Park, M. Kim, J. H. Jung, and H. S. Kim, "Load adaptive modulation method for all-metal induction heating application," *Conf. Proc. - IEEE Appl. Power Electron. Conf. Expo. - APEC*, vol. 2018-March, pp. 3486–3490, 2018, doi: 10.1109/APEC.2018.8341606.
17. H. Sarnago, O. Lucia, and J. M. Burdio, "Multiple-output ZCS resonant inverter for multi-coil induction heating appliances," *Conf. Proc. - IEEE Appl. Power Electron. Conf. Expo. - APEC*, pp. 2234–2238, 2017, doi: 10.1109/APEC.2017.7931010.
18. O. Lucia, C. Carretero, D. Palacios, D. Valeau, and J. M. Burdío, "Configurable snubber network for efficiency optimisation of resonant converters applied to multi-load induction heating," *Electron. Lett.*, vol. 47, no. 17, pp. 989–991, 2011, doi: 10.1049/el.2011.1711.
19. M. S. Huang, C. C. Liao, Z. F. Li, Z. R. Shih, and H. W. Hsueh, "Quantitative Design and Implementation of an Induction Cooker for a Copper Pan," *IEEE Access*, vol. 9. pp. 5105–5118, 2021, doi: 10.1109/ACCESS.2020.3046713.
20. S. H. Jeong, J. Il Jin, H. P. Park, and J. H. Jung, "Enhanced load adaptive modulation of induction heating series resonant inverters to heat various-material vessels," *J. Power Electron.*, vol. 22, no. 6, pp. 1020–1032, 2022, doi: 10.1007/s43236-022-00409-x.
21. W. Han, K. T. Chau, W. Liu, X. Tian, and H. Wang, "A Dual-Resonant Topology-Reconfigurable Inverter for All-Metal Induction Heating," *IEEE J. Emerg. Sel. Top. Power Electron.*, vol. 10, no. 4, pp. 3818–3829, 2022, doi: 10.1109/JESTPE.2021.3071700.
22. S. R. Ramalingam, C. S. Boopthi, S. Ramasamy, M. Ahsan, and J. Haider, "Induction heating for variably sized ferrous and non-ferrous materials through load modulation," *Energies*, vol. 14, no. 24, 2021, doi: 10.3390/en14248354.

23. J. Jin, M. Kim, J. Han, K. Kang, and J. H. Jung, "Input voltage selection method of half-bridge series resonant inverters for all-metal induction heating applications using high turn-numbered coils," *J. Power Electron.*, vol. 20, no. 6, pp. 1629–1637, 2020, doi: 10.1007/s43236-020-00147-y.
24. E. Jang, S. M. Park, D. Joo, H. M. Ahn, and B. K. Lee, "Analysis and Comparison of Topological Configurations for All-Metal Induction Cookers," *J. Electr. Eng. Technol.*, vol. 14, no. 6, pp. 2399–2408, 2019, doi: 10.1007/s42835-019-00292-w.
25. H. Sarnago, Ó. Lucía, A. Mediano, and J. M. Burdío, "Analytical Model of the Half-Bridge Series Resonant Inverter for Improved Power Conversion Efficiency and Performance," *IEEE Trans. Power Electron.*, vol. 30, no. 8, pp. 4128–4143, 2015, doi: 10.1109/TPEL.2014.2359576.
26. H. I. Hsieh, C. C. Kuo, and W. Te Chang, "Study of half-bridge series-resonant induction cooker powered by line rectified DC with less filtering," *IET Power Electron.*, 2023, doi: 10.1049/pel2.12503.
27. H. Sarnago, P. Guillén, J. M. Burdío, and O. Lucia, "Multiple-Output ZVS Resonant Inverter Architecture for Flexible Induction Heating Appliances," *IEEE Access*, vol. 7, pp. 157046–157056, 2019, doi: 10.1109/ACCESS.2019.2950346.
28. H. W. Koertzen, J. D. van Wyk, and J. A. Ferreira, "Design of the half-bridge, series resonant converter for induction cooking," *PESC Rec. - IEEE Annu. Power Electron. Spec. Conf.*, vol. 2, pp. 729–735, 1995, doi: 10.1109/pesc.1995.474899.
29. N. Altintas, M. Ozturk, and U. Oktay, "Performance evaluation of pan position methods in domestic induction cooktops," *Electr. Eng.*, 2023, doi: 10.1007/s00202-023-01837-z.
30. I. Hirota, H. Omori, K. A. Chandra, and M. Nakaoka, "Practical evaluations of single-ended load-resonant inverter using application-specific IGBT and driver IC for induction-heating appliance," in *Proceedings of 1995 International Conference on Power Electronics and Drive Systems. PEDS 95*, pp. 531–537, doi: 10.1109/PEDS.1995.404866.
31. I. Sheikhian, N. Kaminski, S. Voß, W. Scholz, and E. Herweg, "Optimisation of Quasi-resonant Induction Cookers," *2013 15th Eur. Conf. Power Electron. Appl. EPE 2013*, 2013, doi: 10.1109/EPE.2013.6631837.
32. M. Ozturk and N. Altintas, "Multi-output AC–AC converter for domestic induction heating," *Electr. Eng.*, vol. 105, no. 1, pp. 297–316, Feb. 2023, doi: 10.1007/s00202-022-01664-8.
33. J. Villa, D. Navarro, A. Dominguez, J. I. Artigas, and L. A. Barragan, "Vessel Recognition in Induction Heating Appliances - A Deep-Learning Approach," *IEEE Access*, vol. 9. pp. 16053–16061, 2021, doi: 10.1109/ACCESS.2021.3052864.
34. E. Spateri, F. Ruiz, and G. Gruosso, "Modelling and Simulation of Quasi-Resonant Inverter for Induction Heating under Variable Load," *Electron.*, vol. 12, no. 3, 2023, doi: 10.3390/electronics12030753.
35. Zheng-Feng Li, Jhih-Cheng Hu, Ming-Shi Huang, Yi-Liang Lin, Chun-Wei Lin, and Yu-Min Meng, "Load Estimation for Induction Heating Cookers Based on Series RLC Natural Resonant Current." doi: 10.3390/en15041294.
36. H. Sarnago, O. Lucía, and J. M. Burdio, "A Versatile Resonant Tank Identification Methodology for Induction Heating Systems," *IEEE Trans. Power Electron.*, vol. 33, no. 3, pp. 1897–1901, Mar. 2018, doi: 10.1109/TPEL.2017.2740998.
37. J. Acero, J. M. Burdío, L. A. Barragán, and R. Alonso, "A model of the equivalent impedance of the coupled winding-load system for a domestic induction heating application," *IEEE Int. Symp. Ind. Electron.*, no. 1, pp. 491–496, 2007, doi: 10.1109/ISIE.2007.4374646.
38. J. Acero, O. Lucia, C. Carretero, I. Lope, and C. Diez, "Efficiency improvement of domestic induction appliances using variable inductor-load distance," in *2012 Twenty-Seventh Annual IEEE Applied Power Electronics Conference and Exposition (APEC)*, Feb. 2012, pp. 2153–2158, doi: 10.1109/APEC.2012.6166119.
39. H. Okuno, H. Yonemori, and M. Kobayashi, "Relation of gap length and resonant frequency about a double-coil drive type IH cooker," in *2008 15th IEEE International Conference on Electronics, Circuits and Systems*, Aug. 2008, pp. 65–68, doi: 10.1109/ICECS.2008.4674792.
40. P. Charoenwiangnuea, C. Ekkaravarodome, I. Boonyaroonate, P. Thounthong, and K. Jirasereeamornkul, "Design of domestic induction cooker based on optimal operation class-E inverter with parallel load network under large-signal excitation," *J. Power Electron.*, vol. 17, no. 4, pp. 892–904, 2017, doi: 10.6113/JPE.2017.17.4.892.
41. P. Charoenwiangnuea, S. Wangnipparnto, and S. Tunyasrirut, "Design of A Class-E Direct AC-AC Converter with Only One Capacitor and One Inductor for Domestic Induction Cooker," in *2021 18th*

International Conference on Electrical Engineering/Electronics, Computer, Telecommunications and Information Technology (ECTI-CON), May 2021, pp. 679–682, doi: 10.1109/ECTI-CON51831.2021.9454917.

42. S. Yilmaz, B. S. Sazak, and S. Cetin, "Design and implementation of web-based training tool for a single switch induction cooking system using PHP," *Elektron. ir Elektrotechnika*, no. 3, pp. 89–92, 2010, [Online]. Available: https://www.semanticscholar.org/paper/Design-and-Implementation-of-Web-Based-Training-for-Yilmaz-Sazak/d44d3831c3d6722cf80422afd7a4eabaf1f091f9.
43. B. S. Sazak, "Design of a 500W Resonant Induction Heater," *Pamukkale Univ. J. Eng. …*, pp. 1–12, 2011, [Online]. Available: https://www.researchgate.net/publication/267858491_DESIGN_OF_A_500W_RESONANT_INDUCTION_HEATER.
44. H. Zeroug, T. M. Leulmi, M. M. Lograda, and N. Tadrist, "Design and development of IGBT resonant inverters for domestic induction heating applications," in *6th IET International Conference on Power Electronics, Machines and Drives (PEMD 2012)*, 2012, pp. F22–F22, doi: 10.1049/cp.2012.0360.
45. L. Meng, K. Wai, E. Cheng, S. Member, and K. W. Chan, "Systematic Approach to High-Power and Energy-Efficient Industrial Induction Cooker System : Circuit Design , Control Strategy , and Prototype Evaluation," vol. 26, no. 12, pp. 3754–3765, 2011.
46. H. Terai *et al.*, "Comparative Performance Evaluations of IGBTs and MCT in Single-Ended Quasi-Resonant Zero Voltage Soft Switching Inverter," no. 1, pp. 2178–2182.
47. H. Omori, H. Yamashita, M. Nakaoka, and T. Maruhashi, "A novel type induction-heating single-ended resonant inverter using new bipolar Darlington-Transistor," in *1985 IEEE Power Electronics Specialists Conference*, Jun. 1985, pp. 590–599, doi: 10.1109/PESC.1985.7070998.
48. I. Millán, D. Puyal, J. M. Burdío, O. Lucía, and C. M. De Luna, "IGBT Selection Method for the Design of Resonant Inverters for Domestic Induction Heating Keywords Method to measure the power losses," vol. 1.
49. J. Acero *et al.*, "The domestic induction heating appliance: An overview of recent research," in *2008 Twenty-Third Annual IEEE Applied Power Electronics Conference and Exposition*, Feb. 2008, pp. 651–657, doi: 10.1109/APEC.2008.4522791.
50. T. Nishida, S. Moisseev, E. Hiraki, and M. Nakaoka, "Duty Cycle Controlled Soft Combutation High Frequency Inverter for Consumer Induction Cooker and Steaimer," pp. 1846–1851, 1846.
51. V. Crisafulli and M. Antretter, "Design considerations to increase power density in induction cooking applications using the new Field stop II technology IGBTs," *PCIM Eur. 2015; Int. Exhib. Conf. Power Electron. Intell. Motion, Renew. Energy Energy Manag. Proc.*, no. May, pp. 19–21, 2015.
52. M. N. O. S. Charles K. Alexander, *Fundamentals of Electric Circuits*, 7th Editio. McGraw-Hill Education,.